Available online at www.sciencedirect.com
SCIENCE DIRECT
Cement and Concrete Research 36 (2006) 1076–1082
Cement and Concrete Research

# Monte Carlo simulation of electron-solid interactions in cement-based materials

H.S. Wong *, N.R. Buenfeld

*Concrete Durability Group, Department of Civil and Environmental Engineering, Imperial College London, SW7 2AZ, UK*

Received 10 September 2005; accepted 10 March 2006

**Abstract**

Knowledge of the size of the electron-solid interaction volume and the sampling volume of various signals within it is important for interpretation of images and analytical results obtained from electron microscopy. In this study we used a Monte Carlo technique to simulate electron trajectories in order to investigate the shape and size of the interaction volume, the spatial and energy distribution of backscattered electrons and characteristic X-rays in cement-based materials. We found that the maximum penetration depth of the electron trajectories ranges from 0.75 to 1.5 μm at 10 keV and from 2.5 to 5.0 μm at 20 keV. For backscattered electrons, the maximum sampling depth is about 30% of the interaction volume depth and its lateral dimension is close to the interaction volume depth. The sampling volume size of characteristic X-rays is a substantial fraction of the interaction volume. For ettringite, the amount of material analysed in X-ray microanalysis is in the order of 1 to 100 $\mu m^3$ at conventional SEM accelerating voltages of 10 to 20 keV.


*Keywords:* Backscattered electron imaging; EDX; Image analysis; Microstructure; SEM; Monte Carlo simulation

## 1. Introduction

Electron microscopy, in particular the backscattered electron (BSE) mode coupled with X-ray microanalysis, is an important research tool in cement and concrete science. For many years, electron microscopy has been used for qualitative and quantitative studies of the microstructure and chemical composition of phases in cement-based materials. In this journal alone, an electronic search [1] using the keywords electron microscopy, SEM, EDS or EDX returned more than 500 articles within the abstract, title or keywords field and more than 1500 articles within the full-text field, dating from its first publication in 1971.

In the electron microscope, a high energy electron probe with a size in the nanometre range is focussed onto a target sample. The interactions between the incident electrons and the sample produce various signals that can be used to form images or spectra, giving information regarding topography, structure and chemical composition of the sample. However, these signals are generated within a finite volume in the sample that can be substantially larger than the incident probe size. Therefore, knowledge of the shape and dimension of this interaction volume, the distribution of various signals within it and factors that control this, are critical for interpretation of the resulting images or spectra.

The shape and size of the interaction volume depend on the sample properties (chemical composition, atomic number, density) and the operating conditions of the electron microscope (accelerating voltage, probe diameter, surface tilt). For cement-based materials, the shape of the interaction volume is generally assumed to follow that of low density, low atomic number materials, i.e. pear shaped with a small entry neck (where most secondary and backscattered electrons originate). As electrons penetrate deeper, the lateral spread of the electron-solid interaction region increases. The lateral dimension of the interaction volume for cement-based materials is thought to be around 1–2 μm [2] and the volume of the material analysed by the electron probe is approximately 1–2 $\mu m^3$ [3].

In this study we will use a Monte Carlo technique to simulate the electron-solid interactions in cement-based materials. Our aim is to investigate the shape and size of the interaction volume in

* Corresponding author. Tel.: +44 20 7594 5957; fax: +44 20 7225 2716.
*E-mail address:* hong.wong@imperial.ac.uk (H.S. Wong).

0008-8846/$ - see front matter © 2006 Elsevier Ltd. All rights reserved.
doi:10.1016/j.cemconres.2006.03.006

cement-based materials under typical microscope operating conditions. The particular focus will be the region where backscattered electrons and characteristic X-rays are generated when a flat-polished sample is subjected to conventional beam energies (10–20 keV). We hope that this study will give a better understanding of the signal formation process and the performance and limitations of electron microscopy as an imaging and analytical tool for cement and concrete research. This can also assist in the selection of an optimal imaging strategy for a particular application and facilitate interpretation of results.

## 2. Electron-solid interactions and Monte Carlo simulation

This section gives a brief overview on the physical processes that occur when an electron beam interacts with a solid target and how Monte Carlo methods can be used to simulate this. A detailed mathematical description is beyond the scope of this paper; however, comprehensive treatment of the subject can be found in Refs. [4–6].

When a beam of high-energy electrons hits a solid target, the electrons will interact with the electrical fields of the target's atoms and undergo elastic and inelastic scattering events. In elastic scattering, the incident electron is deflected to a new trajectory with no energy loss. After several elastic scattering events, the electrons will spread out and some may escape the sample surface as backscattered electrons. The incident electrons will also gradually lose their energy with distance travelled via inelastic scattering. Kinetic energy is transferred to the sample, producing signals such as secondary electrons, auger electrons, cathodoluminescence, and characteristic and continuum X-rays. There are several mathematical models that describe the probability of an electron undergoing elastic scattering, most notably the Rutherford and Mott scattering cross-section [7]. For inelastic scattering, the Bethe's stopping power equation [8] describes the rate of energy loss with distance travelled.

Apart from low atomic number materials such as polymethylmethacrylate that undergoes damage during electron bombardment, experimental observation of the interaction volume for higher atomic number materials is not possible. As a result, the Monte Carlo simulation technique has been developed over the last four decades to study electron-solid interactions and is now an established tool for interpretation of SEM images and X-ray microanalysis results. Specifically, the Monte Carlo method can simulate the angular, lateral and depth distributions of secondary, backscattered and transmitted electrons, energy dissipation and generation of characteristic X-rays [9–14]. These are used to determine the spatial resolution for each signal for a particular operating condition and sample composition. Recent applications include studies of the resolution in semiconductor multilayers [15] and the position of phase boundaries in composite materials [16].

In a Monte Carlo simulation, the electron trajectory is followed in a stepwise manner from its entry point until it loses all of its energy and is absorbed, or until the electron is backscattered. At each point, the probability of the electron undergoing scattering, the scattering angle, distance between scattering events and the rate of energy loss is calculated from appropriate physical models. The location of the electron within the sample and its kinetic energy is constantly updated with time, together with the generation of secondary electrons and characteristic X-rays. Fig. 1 shows an example of a Monte Carlo simulation of electron trajectories at 20 keV accelerating voltage in a calcium hydroxide target.

Since electron-solid interaction is essentially a stochastic process, random numbers and weighing factors are used to replicate the statistical distribution of scattering events, hence the name 'Monte Carlo'. Therefore, the accuracy of the simulation depends entirely on the models and assumptions used, but knowledge of these has been built over the years of improvements to the approximations adopted to describe the elastic and inelastic scatterings. The accuracy and limits of applicability of Monte Carlo simulations have been established by comparison with experimental values, for example in Refs. [12,17].

## 3. Experimental

For the simulation, we use CASINO (Version 2.42), which is the acronym for monte CArlo SImulation of electroN trajectory in sOlid, developed by Professor Dominique Drouin and his colleagues at Université de Sherbrooke. This programme is specifically designed for a low energy beam interaction in bulk or thin samples, and can be used to generate backscattered electrons and characteristic X-rays either as a point analysis or as a line-

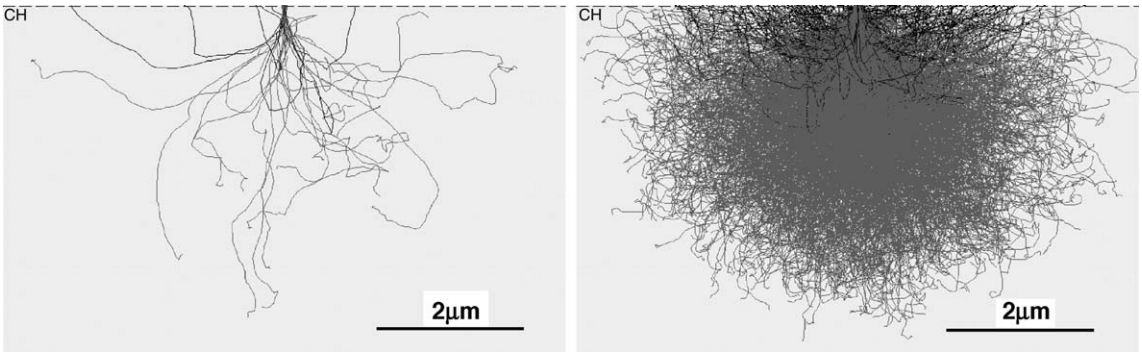


Fig. 1. Simulation of 25 electron trajectories (left) and $2 \times 10^3$ electron trajectories (right) in calcium hydroxide at 20 keV. Elastic scattering occurs where the electron changes direction. The electron trajectory is followed until it loses all of its energy (grey lines) or is backscattered (black lines). For each trajectory, the spatial location, energy distribution and generated X-rays are tracked.

scan for accelerating voltages between 0.1 and 30 keV. A detailed description of the programme is available in Refs. [18–20].

Table 1 provides the major phases in cement-based materials. To create a simulation for a particular phase, the chemical composition, density, weight fraction and atomic fraction of each element is first defined. Then, the microscope settings: accelerating voltage (5–30 keV), angle of the incident beam (0°, i.e. normal to the sample surface), probe diameter and take-off angle of the X-ray detector (40°) are defined. The probe diameter is calculated from the brightness and threshold equation, and corrected for lens aberrations for a conventional tungsten filament electron source, according to the method described by Goldstein et al. [4]. The probe diameters are listed in Table 2. In the calculations, we assumed that the microscope is set up to image an atomic number contrast level $C$ $(=(\eta_2-\eta_1)/\eta_2\times 100)$ of 2.5% with a detector collection efficiency of 0.1 and scan time of 100 s for a $1024\times768$ image; thus a probe current greater than 0.5 nA must be applied. According to the Rose visibility criterion ($\Delta S>5N$), at this imaging condition, the epoxy-filled voids, hydrated cement paste (Aft, Afm, C-S-H), calcium hydroxide and ferrite can be differentiated from their brightness intensity, which is generally observed in routine BSE imaging. We note that the uncertainties in the assumptions made in calculating brightness and lens aberrations can lead to an error of several hundred percent in the final effective probe diameter. However, in the results section, we show that this does not make a significant difference to the simulated results for most practical situations.

Finally, the physical model, number of simulated electrons and the minimum energy to which the trajectory is followed, is selected. We used the Mott model for elastic scattering and the modified Bethe equation [21] to model the deceleration and energy loss. A large number of electron trajectories must be calculated in order to statistically replicate the physical processes involved. We calculated $4\times10^5$ electron trajectories for each simulation. This value was derived from the probe current and pixel dwell time. As a rule of thumb, the estimate of relative error is $1/\sqrt{n}$, where $n$ is the number of electrons simulated. Hence, for a simulation of $4\times10^5$ electrons, the relative error is about 0.2%. The trajectory of each electron is followed until its energy falls below 0.5 keV, or until the electron has returned to the sample surface. In the simulation, we assumed that each phase is stoichiometric, dense, topography-free and homogeneous in composition over the entire interaction volume.

Table 2
Calculated values of brightness ($\beta$), Gaussian probe diameter ($d_{min}$), chromatic aberration ($d_c$), spherical aberration ($d_s$), aperture diffraction ($d_d$) and effective probe diameter ($d_p$) at several accelerating voltages ($E$)

| $E$ (keV) | $\beta$ (A/m$^2$ .sr) | $d_{min}$ (nm) | $d_c$ (nm) | $d_s$ (nm) | $d_d$ (nm) | $d_p$ (nm) |
|---|---|---|---|---|---|---|
| 5 | $2.7\times10^8$ | 177 | 20 | 1.3 | 2.1 | 178 |
| 10 | $5.4\times10^8$ | 125 | 10 | 1.3 | 1.5 | 126 |
| 15 | $8.2\times10^8$ | 102 | 7 | 1.3 | 1.2 | 102 |
| 20 | $1.1\times10^9$ | 88 | 5 | 1.3 | 1.1 | 89 |
| 25 | $1.4\times10^9$ | 79 | 4 | 1.3 | 1.0 | 79 |
| 30 | $1.6\times10^9$ | 72 | 3 | 1.3 | 0.9 | 72 |

## 4. Results

### 4.1. Verification of the Monte Carlo code

The accuracy of the Monte Carlo code was tested by comparing the simulated backscatter coefficients (i.e. the ratio of backscattered electrons to the total simulated trajectories) with experimentally measured values or with calculated values. Fig. 2 shows the results for all elements between Li and Ca in the periodic table, and for the main phases in cement-based materials (Table 1). The experimental values were obtained from a list compiled by Joy [22] of known experimentally measured secondary and backscattered electron coefficients, and electron stopping power data for elements and compounds. The calculated backscatter coefficients were from the empirical equation proposed by Reuter [23], which was obtained by curve-fitting to Heinrich's [24] experimental data at 20 keV:

$$\eta = -0.0254 + 0.016Z - 1.86\times10^{-4}Z^2 + 8.3\times10^{-7}Z^3 \quad (1)$$

where $\eta$ is the backscatter coefficient and $Z$ is the atomic number. For a compound, the mean backscatter coefficient is calculated using Castaing's rule [25], i.e. summation of each constituent

Table 1
Major phases in cement-based materials arranged according to increasing backscatter coefficient

| Phase | Molecular wt. | Atomic no. | Mean atomic no. | Density (g/cm$^3$) | Backscatter coefficient, $\eta$ | Contrast, % |
|---|---|---|---|---|---|---|
| Epoxy (Araldite), $C_{10}H_{18}O_4$ | 202.250 | 110 | 6.184 | 1.14 | 0.066 | – |
| Brucite, $Mg(OH)_2$ | 58.326 | 30 | 9.423 | 2.39 | 0.109 | 39.1 |
| Thaumasite, $CaSiO_3{\cdot}CaSO_4{\cdot}CaCO_3{\cdot}15H_2O$ | 622.616 | 326 | 10.622 | 1.89 | 0.120 | 9.7 |
| Ettringite, $3CaO{\cdot}Al_2O_3{\cdot}3CaSO_4{\cdot}32H_2O$ | 1254.648 | 658 | 10.769 | 1.70 | 0.122 | 1.5 |
| Dolomite, $CaMg(CO_3)_2$ | 184.408 | 92 | 10.875 | 2.84 | 0.124 | 1.4 |
| Quartz, $SiO_2$ | 60.066 | 30 | 10.806 | 2.62 | 0.125 | 1.3 |
| Monosulphate, $3CaO{\cdot}Al_2O_3{\cdot}CaSO_4{\cdot}12H_2O$ | 622.320 | 322 | 11.665 | 1.99 | 0.132 | 5.3 |
| Calcium silicate hydrate, $C_{1.7}$-S-$H_4$ | 227.460 | 118 | 12.086 | 2.12 | 0.137 | 3.5 |
| Gypsum, $CaSO_4{\cdot}2H_2O$ | 172.170 | 88 | 12.119 | 2.32 | 0.138 | 0.6 |
| Calcite, $CaCO_3$ | 100.088 | 50 | 12.563 | 2.71 | 0.142 | 2.9 |
| Portlandite, $Ca(OH)_2$ | 74.076 | 38 | 14.302 | 2.24 | 0.162 | 12.1 |
| Tricalcium aluminate, $3CaO{\cdot}Al_2O_3$ | 270.198 | 134 | 14.339 | 3.21 | 0.164 | 1.3 |
| Dicalcium silicate, $2CaO{\cdot}SiO_2$ | 172.250 | 86 | 14.562 | 3.28 | 0.166 | 1.4 |
| Tricalcium silicate, $3CaO{\cdot}SiO_2$ | 228.330 | 114 | 15.057 | 3.03 | 0.172 | 3.1 |
| Ferrite, $4CaO{\cdot}Al_2O_3{\cdot}Fe_2O_3$ | 485.980 | 238 | 16.651 | 3.73 | 0.186 | 7.8 |

Atomic contrast is calculated from the backscatter coefficients of successive phases.

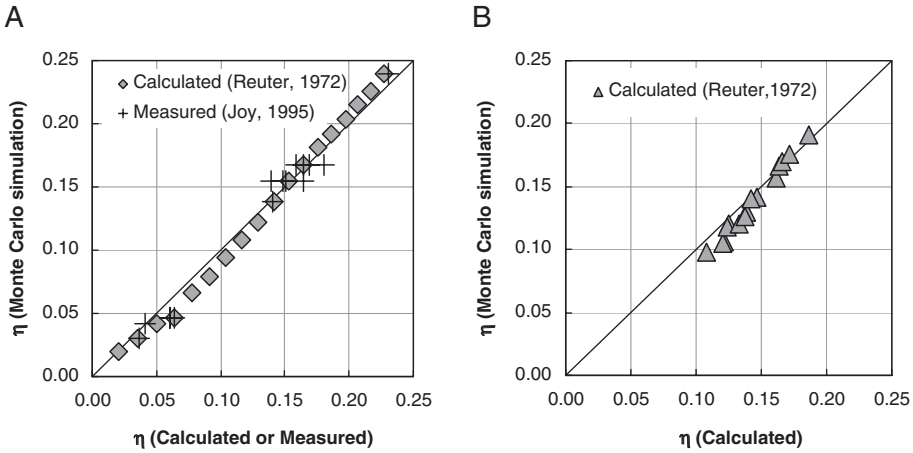


Fig. 2. Testing the accuracy of the Monte Carlo simulation by comparing the simulated and experimentally measured [22] or calculated [23] BSE coefficients for A) all elements between Li and Ca in the periodic table; and B) main phases in cement-based materials (see Table 1).

element's backscatter coefficient, factored by the atomic weight fraction $c_i$:

$$\bar{\eta} = \sum_{i=1}^{n} c_i \eta_i \quad (2)$$

Generally, the simulated backscatter coefficients were in good agreement with the experimental and calculated values for elements ($Z=3-20$) and for the main phases in cement-based materials ($\bar{Z}=6-17$). For each phase, five repeat simulations were made to calculate the average backscatter coefficient, and the coefficients of variation for all values were smaller than 1%. This shows that there is no statistically significant difference between different simulations for a given set of input parameters because a very large number of electrons were simulated each time. Therefore, a repeat simulation is not essential.

### 4.2. Effect of accelerating voltage and probe diameter

Figs. 3 and 4 show the influence of accelerating voltage and probe diameter on the maximum penetration depth of all electrons, i.e. the maximum depth of each trajectory from the surface, and the surface radius of backscattered electrons, in a calcium hydroxide target. The results show that the interaction volume is a strong function of the electron beam energy, and this is well known [4]. The results also show that an order of magnitude change in the calculated probe diameter (Table 2) does not have a significant effect on the penetration depth and backscattered electron escape surface radius. This is because, at 10–20 keV accelerating voltages, the interaction volume for cement-based materials is significantly larger than the probe diameter. However, at low accelerating voltages, the probe diameter becomes critical to the backscattered electron surface radius when its dimension approaches that of the escape surface radius.

### 4.3. Depth of the interaction volume

Fig. 5 shows the cumulative distribution of the penetration depth of all electron trajectories at 10 and 20 keV for ferrite ($C_4AF$), tricalcium silicate ($C_3S$), calcite ($CaCO_3$), calcium hydroxide (CH), calcium silicate hydrate (C-S-H), monosulphate (Afm) and ettringite (Aft). The maximum penetration depth

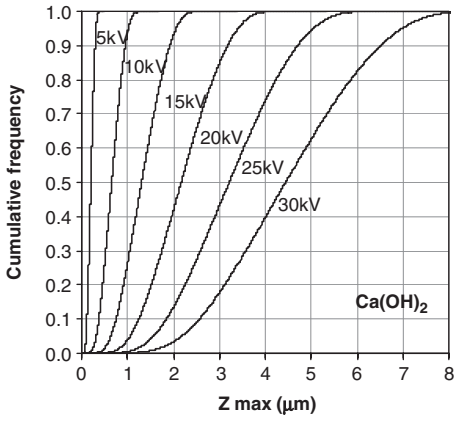


Fig. 3. Effect of accelerating voltage on the maximum penetration depth of electron trajectories in calcium hydroxide.

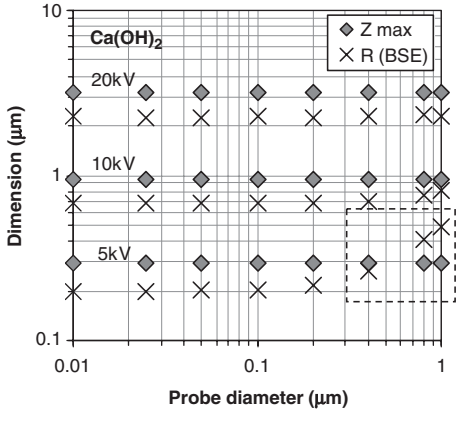


Fig. 4. Effect of probe diameter on the 90th percentile maximum penetration depth ($Z_{max}$) of all electrons and surface radius ($R_{BSE}$) of backscattered electrons for calcium hydroxide at accelerating voltages of 5, 10 and 20 kV.

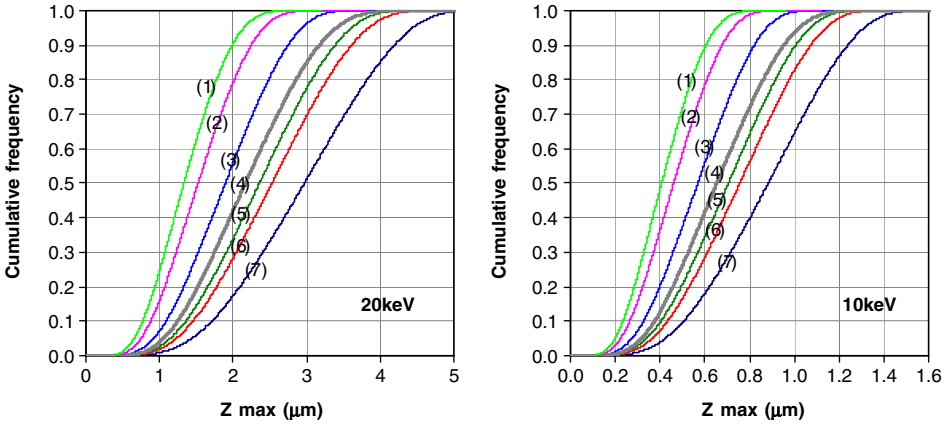


Fig. 5. Cumulative distribution of penetration depth of electrons at 20 and 10 keV accelerating voltage for selected phases: 1) $C_4AF$; 2) $C_3S$; 3) $CaCO_3$; 4) CH; 5) C-S-H; 6) Afm; and 7) Aft.

range is 0.75–1.5 μm at 10 keV and 2.5–5.0 μm at 20 keV accelerating voltage. At a constant beam energy, the depth of the interaction volume generally increases with a decrease in mean atomic number and density. The shape of the interaction volume for all phases follows closely that is shown in Fig. 1 for CH, and appears to be more spherical than pear-shaped.

### 4.4. Sampling volume of backscattered electrons

Fig. 6 shows the distribution of penetration depth and escape surface radius of backscattered electrons for ferrite, calcium hydroxide and ettringite at 10 and 20 keV. These phases were selected because they cover the range of mean atomic number in cement-based materials. The sampling depth of backscattered electrons at 90th percentile ranges from 0.23 to 0.46 μm at 10 keV and from 0.76 to 1.6 μm at 20 keV. This is approximately 30% of the interaction volume depth. The escape surface radius at 90th percentile ranges from 0.43 to 0.87 μm at 10 keV and from 1.4 to 2.9 μm at 20 keV. Thus, the lateral dimension of the BSE sampling volume is almost equivalent to the depth of the entire interaction volume.

The simulations show that incident electrons can penetrate the sample and emerge at a significant distance from the electron probe impact point, particularly for high beam energies. A large sampling volume and lateral spreading of the backscattered electrons reduces the sensitivity of BSE imaging to fine surface details. However, it may be argued that not all backscattered electrons that escape from the sample surface may generate a response in the detector and contribute to the final image intensity because conventional backscatter detectors are sensitive to high energy backscattered electrons only. Since electrons that travel deeper into the sample and escape further from the probe impact point are likely to have lost a substantial amount of energy via inelastic scattering, these low-energy backscattered electrons may not have a significant contribution to the final image.

Fig. 7 shows the energy distribution of all backscattered electrons for ferrite, calcium hydroxide and ettringite at 10 and 20 keV. According to Goldstein et al. [4], the energy threshold for a typical solid-state detector is in the range of 2 to 5 keV. Taking a conservative estimate of 5 keV, we find that the amount of 'detected' backscattered electrons is still a substantial fraction of the entire population: approximately 95% at 20 keV and 70% at 10 keV.

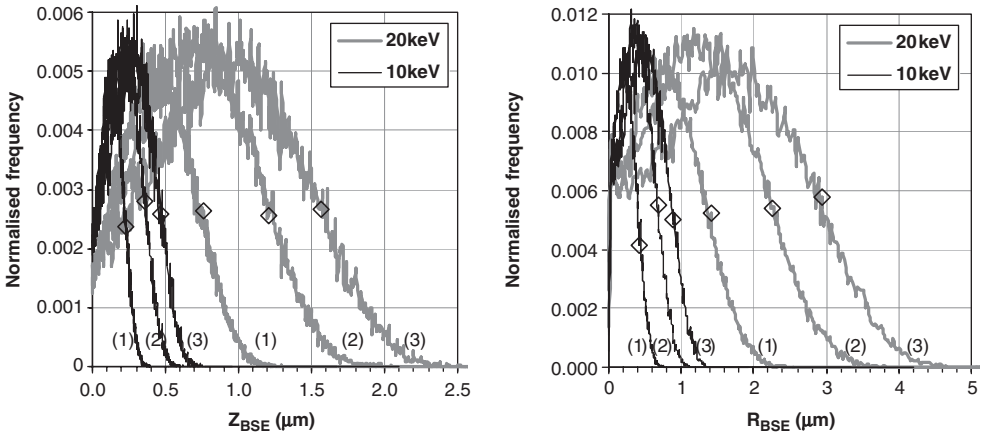


Fig. 6. Distribution of penetration depth ($Z_{BSE}$) and escape surface radius ($R_{BSE}$) of backscattered electrons at 20 and 10 keV accelerating voltage for selected phases: 1) $C_4AF$; 2) CH; and 3) Aft. The symbol (◇) marks the 90th cumulative percentile.

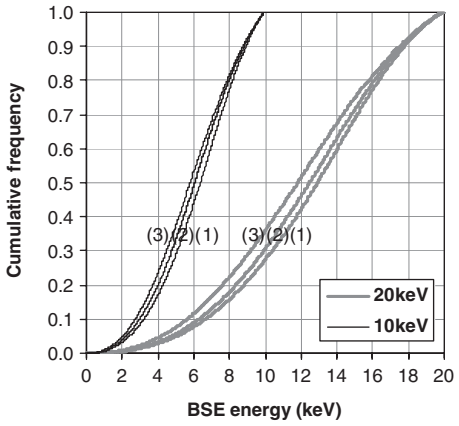


Fig. 7. Cumulative distribution of backscattered electron energy at 20keV and 10keV accelerating voltage for selected phases: 1) $C_4AF$; 2) CH; and 3) Aft.

### 4.5. Sampling volume of characteristic X-rays

Ettringite may play an important role in concrete degradation and because X-ray microanalysis is a conventional technique used for its detection, we will give a particular attention to this phase in this section.

Characteristic X-rays may be generated anywhere within the interaction volume, as long as the incident electron energy exceeds the critical excitation energy of the particular element present. For ettringite, the critical excitation energy for CaLα, OKα, AlKα, SKα and CaKα is 0.349, 0.532, 1.560, 2.470 and 4.308 keV respectively [26]. The smaller the critical excitation energy, the larger the sampling volume of the characteristic X-rays for that particular element since incident electrons will progressively lose energy as they penetrate the sample. However, X-rays generated deep in the sample may not escape as a result of photoelectric absorption. This is the process where the entire energy of the X-ray photon is transmitted to an orbital electron of the sample, which is subsequently ejected.

Fig. 8 shows the depth and lateral distribution of the non-absorbed characteristic X-rays in ettringite. As with the case of backscattered electrons, the results show a non-even distribution of X-ray intensity with distance from the probe impact point; the X-ray intensity is highest near the probe impact point and decreases to zero when the electron energy falls below the critical excitation energy. The X-ray sampling volume for each element depends on the electron beam energy and the critical excitation energy, and can be a substantial fraction of the interaction volume. Assuming a semi-hemispherical sampling volume, the amount of material analysed can be in the order of 1 to 100 $\mu m^3$.

## 5. Discussion

Since the size of the signal sampling volume is a strong function of the electron beam energy, a low accelerating voltage should be used to obtain high sensitivity to fine surface features. However, at a low accelerating voltage, the signal-to-noise (S/N) ratio drops significantly and this degrades spatial resolution. For cement-based materials imaged using a conventional electron microscope, the smallest accelerating voltage at an acceptable S/N ratio is around 10 keV. To improve the S/N ratio at lower accelerating voltages, the probe current can be increased by using a larger probe size, but there is a limit to this because, as shown in the simulation results (Fig. 4), the influence of a probe size on the sampling volume will be significant when its dimension approaches that of the sampling volume. The probe current can also be increased by increasing the emission current and this is now possible with field-emission type electron sources that can maintain high probe brightness and current at a very fine probe size and a low accelerating voltage.

The sampling volume of non-absorbed characteristic X-rays is a substantial fraction of the interaction volume. For ettringite, we showed that the volume of the material analysed is estimated to be in the order of 1–100 $\mu m^3$ at 10–20 keV. Therefore, to obtain an accurate quantitative X-ray microanalysis, one should ensure that the point selected for analysis is homogeneous in chemical composition over this volume of material. As in BSE imaging, a low accelerating voltage is preferable. Selecting higher beam energy may increase the total X-ray counts/s, but at the expense of reduced sensitivity. The suitable beam energy to be used for X-ray microanalysis depends on the characteristic

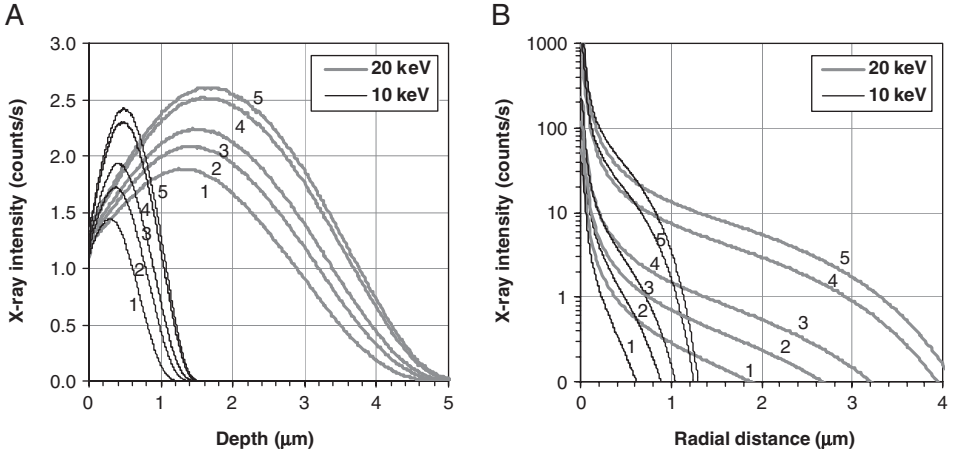


Fig. 8. Depth and lateral distribution of non-absorbed X-rays in Aft at 20keV and 10keV. Symbols: 1) CaKα; 2) SKα; 3) AlKα; 4) OKα and 5) CaLα.

X-rays of interest and the composition of the sample; typically 2–3 times that of the critical excitation energy is the optimal value [4].

## 6. Conclusions

In this study, we applied a Monte Carlo technique to simulate the electron-solid interactions in cement-based materials at accelerating voltages used in conventional SEMs (10–20 keV), in order to study the shape and size of the interaction volume, the spatial and energy distribution of backscattered electrons and non-absorbed characteristic X-rays. We first verified that the Monte Carlo code is applicable for cement-based materials by comparing the simulated backscatter coefficients with the experimental and calculated values. Good agreement was observed for all major phases in cement-based materials. We showed that the size of the interaction volume and sampling volume of backscattered electrons is a strong function of the beam energy, but independent of the probe size. The probe diameter only becomes critical to the backscattered electron escape surface radius when its dimension approaches that of the surface radius at low beam energy (<10 keV).

We observed that the interaction volume in cement-based materials is more hemispherical than pear-shaped. The maximum penetration depth of electron trajectories ranges from 0.75 to 1.5 μm at 10 keV and from 2.5 to 5.0 μm at 20 keV. The distribution of backscattered electrons and characteristic X-rays within this interaction volume is not uniform, but is concentrated near the probe impact point. The maximum sampling depth of backscattered electrons is approximately 30% of the interaction volume depth and its lateral dimension is almost equivalent to the interaction volume depth. The sampling volume of characteristic X-rays for each element depends on the beam energy and the critical excitation energy, and can be a substantial fraction of the interaction volume. For ettringite, the amount of material analysed in X-ray microanalysis is in the order of 1–100 $\mu m^3$ at 10–20 keV.

## Acknowledgements

HSW would like to acknowledge the financial assistance provided by the Universities UK, via the Overseas Research Students Awards Scheme. We thank Professor Dominique Drouin of Université de Sherbrooke, for the advice on CASINO.

## References

[1] ScienceDirect®, http://www.sciencedirect.com, September 2005.
[2] K.L. Scrivener, Backscattered electron imaging of cementitious microstructures: understanding and quantification, Cem. Concr. Compos. 26 (8) (2004) 935–945.
[3] O.M. Jensen, A.M. Coats, F.P. Glasser, Chloride ingress profiles measured by electron probe micro analysis, Cem. Concr. Res. 26 (11) (1996) 1695–1705.
[4] J. Goldstein, D. Newbury, D. Joy, C. Lyman, P. Echlin, E. Lifshin, L. Sawyer, J. Michael, Scanning Electron Microscopy and X-Ray Microanalysis, Third Edition, Kluwer Academic/Plenum Publishers, New York, 2003.
[5] D.C. Joy, Monte Carlo Modelling for Microscopy and Microanalysis, Oxford University Press, New York, 1995.
[6] R. Shimizu, D. Ze-Jun, Monte Carlo modelling of electron-solid interactions, Rep. Prog. Phys. (1992) 487–531.
[7] N.F. Mott, H.S.W. Massey, The Theory of Atomic Collisions, Third edition, Oxford University Press, Oxford, 1965.
[8] H.A. Bethe, Zur theorie des dutchgangs schneller korpuskularstrahlen durch materie, Ann. Phys. (Leipzig) 5 (1930) 325–400.
[9] R. Shimizu, K. Murata, Monte Carlo calculations of the electron-sample interactions in the scanning electron microscope, J. Appl. Phys. 42 (1) (1971) 387–394.
[10] R. Shimizu, T. Ikuta, K. Murata, The Monte Carlo technique as applied to the fundamentals of EPMA and SEM, J. Appl. Phys. 43 (10) (1972) 4233–4249.
[11] K. Murata, Spatial distribution of backscattered electrons in the scanning electron microscope and electron microprobe, J. Appl. Phys. 45 (9) (1974) 4110–4117.
[12] R. Shimizu, T. Ikuta, T.E. Everhart, W.J. DeVore, Experimental and theoretical study of energy dissipation profiles of keV electrons in polymethylmethacrylate, J. Appl. Phys. 46 (4) (1975) 1581–1584.
[13] I. Adesida, R. Shimizu, T.E. Everhart, A study of electron penetration in solids using a direct Monte-Carlo approach, J. Appl. Phys. 51 (11) (1980) 5962–5969.
[14] K.F.J. Heinrich, D.E. Newbury, Electron probe quantitation, Plenum Press, New York, 1991.
[15] P.G. Merli, A. Migliori, M. Nacucchi, D. Govoni, G. Mattei, On the resolution of semiconductor multilayers with a scanning electron microscope, Ultramicroscopy 60 (1995) 229–239.
[16] D.R. Cousens, D.C. Joy, A Monte Carlo study of the position of phase boundaries in backscattered electron images, Scanning 19 (1997) 547–552.
[17] D.E. Newbury, R.L. Myklebust, Monte Carlo electron trajectory calculations of electron interactions in samples with special geometries, in: D.F. Kyser, H. Niedrig, D.E. Newbury, R. Shimizu (Eds.), Electron Beam Interactions with Solids for Microscopy, Microanalysis, and Microlithography, Scanning Electron Microscopy Inc., Chicago, 1984, p. 153.
[18] P. Hovington, D. Drouin, R. Gauvin, CASINO: a new Monte Carlo code in C Language for electron beam interaction — Part I: description of the program, Scanning 19 (1997) 1–14.
[19] P. Hovington, D. Drouin, R. Gauvin, CASINO: a new Monte Carlo code in C Language for electron beam interaction — Part II: tabulated values of the Mott cross section, Scanning 19 (1997) 20–28.
[20] P. Hovington, D. Drouin, R. Gauvin, D.C. Joy, N. Evans, CASINO: a new Monte Carlo code in C Language for electron beam interaction — Part III: stopping power at low energies, Scanning 19 (1997) 29–35.
[21] D.C. Joy, S. Luo, An empirical stopping power relationship for low-energy electrons, Scanning 11 (1989) 176–180.
[22] D.C. Joy, A database on electron solid interactions, Scanning 17 (1995) 270–275.
[23] W. Reuter, in: G. Shinoda, K. Kohra, T. Ichinokawa (Eds.), Proc 6th Int Conf X-ray Optics and Microanalysis, Univ. Tokyo Press, Tokyo, 1972, p. 121.
[24] K.F.J. Heinrich, in: R. Castaing, P. Deschamps, J. Philibert (Eds.), X-ray Optics and Microanalysis, 4th Int. Conf. X-Ray Optics and Microanalysis, Hermann, Paris, 1966, p. 1509.
[25] R. Castaing, Electron probe microanalysis, Adv. Electron. Electron Phys. 13 (1960) 317–386.
[26] J.A. Bearden, X-ray wavelengths, Rev. Mod. Phys. 39 (1967) 78–124.